Pharmacological Repression of PPARγ Promotes Osteogenesis

David P. Marciano, **Dana S. Kuruvilla**, **Siddaraju V. Boregowda**, **Alice Asteian**, **Travis S. Hughes**, **Ruben Garcia-Ordonez**, **Cesar A. Corzo**, **Tanya M. Khan**, **Scott J. Novick**, **HaJeung Park**, **Douglas J. Kojetin**, **Donald G. Phinney**, **John B. Bruning**[#], **Theodore M. Kamenecka**, and **Patrick R. Griffin**

Departments of Molecular Therapeutics, The Scripps Research Institute, Scripps Florida, Jupiter, FL33458, USA

[#]School of Molecular and Biomedical Science, The University of Adelaide, Adelaide, Australia 5005

Abstract

The nuclear receptor peroxisome proliferator-activated receptor gamma (PPARγ) is the master regulator of adipogenesis and the pharmacological target of the thiazolidinedione (TZD) class of insulin sensitizers. Activation of PPARγ by TZDs promotes adipogenesis at the expense of osteoblast formation, contributing to their associated adverse effects on bone. Recently we reported the development of PPARγ antagonist SR1664, designed to block the obesity induced phosphorylation of serine 273 (S273) in the absence of classical agonism, to derive insulin sensitizing efficacy with improved therapeutic index. Here we identify the structural mechanism by which SR1664 actively antagonizes PPARγ, and extend these findings to develop the inverse agonist SR2595. Treatment of isolated bone marrow derived mesenchymal stem cells (MSCs) with SR2595 promotes induction of osteogenic differentiation. Together these results identify the structural determinants of ligand mediated PPARγ repression, and suggest a therapeutic approach to promote bone formation.

Keywords

nuclear receptor; antagonist; inverse agonist; PPARγ; adipogenesis; osteoporosis; osteoblast; bone; SR1664; SR2595

Introduction

Central to the lineage commitment of multipotent MSCs is the nuclear receptor PPARγ, the master regulator of adipogenesis and the pharmacological target of the thiazolidinedione (TZD) class of insulin sensitizers[1]. Activation of PPARγ by the TZDs promotes adipocyte differentiation at the expense of osteoblast formation, contributing to their associated adverse effects on bone[2]. To address these concerns, a novel class of partial agonist selective PPARγ modulators (SPPARγMs) were developed that display reduced expression of PPARγ target genes, while maintaining potent insulin sensitizing efficacy similar to that of full agonist TZDs[3]. SPPARγMs demonstrate the ability to decouple PPARγ activation and insulin sensitizing efficacy, while showing improvement for several TZD associated adverse effects in animal models of diabetes[4].

Recently it was demonstrated that the obesity-induced phosphorylation of PPARγ at Serine 273 (pS273) leads to repression of a subset of the receptors' target genes associated with insulin resistance[5]. The efficacy of SPPARγMs and TZDs was shown to correlate with their ability to block pS273, leading to normalization of the dysregulated PPARγ target gene set. Based on these findings, an alternative class of high affinity functional selective PPARγ modulators (FSPPARγMs) was developed that effectively block pS273, while avoiding classical Activation Function 2 (AF2) driven receptor activation[6]. SR1664 is a representative compound from this class of PPARγ modulators that was shown *in vivo* to be similarly efficacious at insulin sensitizing as rosiglitazone, with further improvements on adverse effect markers relative to SPPARγMs.

Here we report the structural mechanism by which SR1664 actively antagonizes PPARγ through an AF2 mediated clash, and extend these findings to enable the structure guided design of the inverse agonist SR2595. Consistent with the desirable bone phenotype observed in PPARγ deficient animal models[7], we demonstrate that pharmacological repression of PPARγ promotes osteogenesis in cultured MSCs. SR2595 has sufficient pharmacokinetics to support *in vivo* studies and demonstrates no negative effects on metabolic parameters in 21 day treated C57BL/6 mice. Together these results demonstrate the effect of pharmacological PPARγ repression on MSC lineage commitment, and suggest a therapeutic approach to promote bone formation devoid of adverse effect on metabolic parameters.

Results

Structural Mechanism of PPARγ Active Antagonism

Efforts to develop structure activity relationship (SAR) around the antagonist SR1664 began with an unexpected observation that its R-enantiomer SR1663 (Fig. 1a) is an agonist that potently activates PPARγ as defined in a co-transfection promoter:reporter assay (Fig. 1b). To elucidate the structural mechanism driving this stereospecific functional divergence, co-crystal structures of the PPARγ ligand binding domain (LBD) in complex with SR1664 and SR1663 were both solved to a resolution of 2.3Å (Fig. 1c; Table 1). Structural alignment revealed no significant differences in the overall global conformation of the LBD (RMSD $C_\alpha = 1.14$Å), consistent with previously reported PPARγ co-crystal structures[8]. The ligands

partially overlap with their biphenyl and indole moieties closely aligned. However, the positioning of the nitro substituent diverges with SR1663 making a favorable pi stacking interaction with phenylalanine 282 (F282 PPARγ1 numbering; PPARγ2 F310) on helix 3, while SR1664 exhibits a steric clash with F282 (Fig. 1c). SR1664 binding to the PPARγ LBD resulted in an increased rate of hydrogen/deuterium exchange (HDX) for helix 3 relative to that observed upon binding SR1663, consistent with disruption of intra-helix hydrogen bonding due to the steric clash with F282 (Fig. 1d). Increased NMR resonance line widths indicate SR1664 increases μs-ms dynamics relative to SR1663, both near the clash site (I279) and distal on helix 3 (I296) (Fig. 1e). Mutagenesis of F282 to alanine (F282A) altered the pharmacology of SR1664 on PPARγ activity, acting as an agonist of the mutant receptor in a transcriptional activity assay (Fig. 1f), and differentially displacing nuclear receptor co-repressor 1 (NCoR1) (Fig. 1g). Together these results suggest that SR1664 actively antagonizes PPARγ through a stereo-specific AF2-mediated, F282-dependent clash; and that stereospecificity confers antagonism within the biaryl indole scaffold.

Structure Guided Design of PPARγ Inverse Agonist SR2595

Based on this emerging SAR it was hypothesized that furthering the AF2 clash observed with SR1664, through addition of a bulkier substituent could result in repression of basal receptor activity[9]. Indeed SR2595, substitution of t-butyl for nitro at the para position of SR1664, repressed transactivation in a promoter:reporter assay (Fig. 2a, b; binding affinity for analogs are provided in Supplementary Table 1) and expression of the adipogenic marker fatty acid binding protein 4 (*FABP4*) in differentiating murine preadipocytes below basal levels (Fig. 2c). This inverse agonist SAR was conserved across several optimized analogs of SR2595 including SR10221 (Fig. 2a-c, Supplementary Fig. 1a). Similar to that observed with the antagonist SR1664, mutagenesis of F282A altered the pharmacology of SR2595 to act as an agonist in transactivation, and on displacement of nuclear receptor co-repressor 1 (NCoR1) (Supplementary Fig. 1b, c). HDX kinetics of the PPARγ LBD demonstrated a strong correlation between transactivation and ligand-induced protection of helix 12, a surface of the receptor critical for cofactor interaction and ligand-dependent receptor transactivation (Fig. 2d). NMR resonances for residues proximal to helix 12 (L465 and H466) were observed only for agonists rosiglitazone and SR1663, indicative of multiple conformational sampling by these residues with PPARγ bound to either antagonist SR1664 or inverse agonists SR2595 and SR10221 (Fig. 2e). These findings demonstrate the structural determinants guiding the design of PPARγ inverse agonist SR2595, and provide a pharmacological approach to repress PPARγ activity and block basal adipogenesis.

Pharmacological repression of PPARγ promotes osteogenesis

As PPARγ deficiency in transgenic mouse models results in enhanced bone formation[7], pharmacological repression of the receptor emerges as a therapeutic strategy to phenocopy these desirable osteogenic effects. Treatment of cultured human mesenchymal stem cells (MSCs) with SR2595 induced a statistically significant increase in osteogenic differentiation as measured by calcium phosphatase deposition (Fig. 3a). This was accompanied by increased expression of bone morphogenetic proteins *BMP2* and *BMP6* (Fig. 3b). Similar effects were observed with siRNA mediated PPARγ silencing in human MSCs (Fig. 3c,d),

and together demonstrate that pharmacological PPARγ repression can induce MSC differentiation towards the osteogenic lineage.

The Effect of Pharmacological PPARγ Repression on Metabolic Parameters

The primary concern with the development of repressive PPARγ inverse agonists is whether they will have negative consequences on metabolic parameters, as the TZD class of insulin sensitizers are potent full agonists. These concerns are partly allayed by the findings that insulin sensitizing efficacy can be decoupled from PPARγ activation[10], along with transgenic PPARγ haploinsufficiency resulting in favorable metabolic outcomes[11,12]. To determine if pharmacological PPARγ repression would impair insulin sensitivity, SR2595 was administered chronically to lean C57BL/6J mice for 21 days. The pharmacokinetic properties of SR2595 were sufficient to support once daily oral dosing at 20mg/kg (Supplementary Fig. 2a and 2b, plasma exposure and drug concentration in epidiymal WAT, respectively). Lean C57BL/6J mice treated with SR2595 demonstrated no significant change in insulin sensitivity as determined by insulin tolerance test (Supplementary Fig. 3a), nor fasting insulin levels (Supplementary Fig. 3b). In addition, no change in food consumption or body weight was observed during the treatment period (Supplementary Fig. 3c,d).

Discussion

In summary, we have identified the structural mechanism by which SR1664 actively antagonizes PPARγ, and extended this work to design the inverse agonist SR2595. Similar SAR was first reported with the estrogen receptor antagonist tamoxifen[13], suggesting a broadly applicable strategy for altering the pharmacology of additional SPPARγM scaffolds[14,15]. Further broadening the applicability of these findings is the observation that PPARγ F282 is evolutionarily conserved in several nuclear receptors that form obligate RXRα heterodimers including PPARα, PPARδ, LXRα, LXRβ, and FXR[16]. Applying this SAR to identify natural antagonists and based on the crystal structures of PPARγ in complex with endogenous fatty acids[17], we would predict that esterification of fatty acids with a bulky substituent would mimic the steric clash observed with SR1664. Cyclic phosphatidic acid, a putative endogenous PPARγ antagonist fits this profile[18], further implicating the enzymatic pathways regulating endogenous negative regulators of PPARγ as critical for maintaining metabolic and bone homeostasis.

The therapeutic utility of pharmacological PPARγ repression is further suggested by several studies that apply genetic receptor ablation or covalent PPARγ antagonists GW9662 and T0070907 that demonstrate efficacy in cancer[19–21], obesity[22–24], arterial neointima formation[25], and bone formation[26]. SR2595 has sufficient pharmacokinetic properties to support animal studies, and the closely matched pharmacokinetics of the biaryl indole series described here provides a useful system to probe PPARγ transcriptional activity *in vivo*.

Methods

SR2595

(S)-4'-((5-((1-(4-(tert-butyl)phenyl)ethyl)carbamoyl)-2,3-dimethyl-1H-indol-1-yl)methyl)-[1,1'-biphenyl]-2-carboxylic acid. Commercially available ethyl 2,3-dimethyl-1*H*-indole-5-

carboxylate was *N*-alkylated with commercially available *tert*-butyl 4′-(bromomethyl)biphenyl-2-carboxylate using NaH in DMF. The corresponding ethyl ester was hydrolysed using aqueous NaOH in ethanol to give the acid, which was coupled to (S)-1-(4-(tert-butyl)phenyl)ethan-1-amine hydrochloride (synthesis already described in patent) using 2-(3H-[1,2,3]triazolo[4,5-b]pyridin-3-yl)-1,1,3,3-tetramethylisouronium hexafluorophosphate(V) (HATU) and diisopropylethylamine in CH_2Cl_2 to give the amide. Final deprotection of the *tert*-butyl ester using 30% trifluoroacetic acid in CH_2Cl_2 and purification by flash chromatography (ethyl acetate/hexanes 10–100%) afforded SR2595. Electrospray ionisation coupled with mass spectrometry (ESI-MS; *m/z*): 548 [M+H]$^+$; ^{1}H NMR (400 MHz, dimethylsulphoxide (DMSO)-d$_6$): δ (p.p.m.) 8.59 (d, *J* = 8.0 Hz, 1H), 8.10 (d, *J* = 1.5 Hz, 1H), 8.68 (dd, *J* = 1.0, 7.6 Hz, 1H), 7.63 (dd, *J* = 1.5, 8.5 Hz, 1H), 7.51 (dt, *J* = 1.5, 7.6 Hz, 1H), 7.44 (d, *J* = 8.8 Hz, 1H), 7.40 (dd, *J* = 1.2, 7.6 Hz, 1H), 7.31-7.33 (m, 4H), 7.23 (d, *J* = 8.3 Hz, 2H), 6.98 (d, *J* = 8.3 Hz, 2H), 5.47 (s, 2H), 5.33 (quint, *J* = 7.2 Hz, 1H), 2.32 (s, 3H), 2.28 (s, 3H), 1.26 (s, 9H); ^{13}C NMR (400 MHz, DMSO-d$_6$): δ (p.p.m.) 169.5, 166.5, 148.7, 142.3, 140.4, 139.2, 137.6, 137.3, 134.0, 132.1, 130.8, 130.4, 129.0, 128.5, 127.5, 127.2, 125.9, 125.8, 125.1, 124.8, 120.3, 117.6, 108.7, 107.2, 47.9, 45.6, 40.1, 34.1, 31.1, 22.1, 10.0, 8.8.

SR10221

(S)-2-(5-((5-(((S)-1-(4-(tert-butyl)phenyl)ethyl)carbamoyl)-2,3-dimethyl-1H-indol-1-yl)methyl)-2-chlorophenoxy)propanoic acid. Commercially available 2-chloro-5-methylphenol and methyl-D(+)-lactate gave the methyl (S)-2-(2-chloro-5-methylphenoxy)propanoate by a Mitsunobu reaction, follows by the bromination with N-bromosuccinimide (NBS) and azobisobutyronitrile (AIBN) in CCl$_4$. The corresponding compound was *N*-alkylated with allyl 2,3-dimethyl-1H-indole-5-carboxylate using NaH in DMF. The deprotection of the allyl group by tetrakis(triphenylphosphine)palladium(0) gave the acid, which was coupled to (S)-1-(4-(tert-butyl)phenyl)ethan-1-amine hydrochloride (synthesis already described in patent) using 2-(3H-[1,2,3]triazolo[4,5-b]pyridin-3-yl)-1,1,3,3-tetramethylisouronium hexafluorophosphate(V) (HATU) and diisopropylethylamine in CH_2Cl_2 to give the amide. Final hydrolyse of the methyl ester using aqueous LiOH in THF and purification by flash chromatography (ethyl acetate/hexanes 10–100%) afforded SR10221. Electrospray ionisation coupled with mass spectrometry (ESI-MS; *m/z*): 562 [M+H]$^+$; ^{1}H NMR (400 MHz, dimethylsulphoxide (DMSO)-d$_6$): δ (p.p.m.) 8.57 (d, *J* = 8.1 Hz, 1H), 8.08 (d, *J* = 1.5 Hz, 1H), 7.60 (dd, *J* = 1.8, 8.6 Hz, 1H), 7.36 (d, *J* = 8.6 Hz, 1H), 7.33 (m, 3H), 7.29 (d, *J* = 8.1 Hz, 1H), 6.79 (d, *J* = 1.8 Hz, 1H), 6.34 (dd, *J* = 1.8, 8.1 Hz, 1H), 5.47 (s, 2H), 5.17 (quint, *J* = 7.1 Hz, 1H), 4.78 (quint, *J* = 6.8 Hz, 1H), 2.27 (s, 3H), 2.26 (s, 3H), 1.50 (d, *J* = 6.8 Hz, 3H), 1.47 (d, *J* = 7.1 Hz, 3H), 1.26 (s, 9H); ^{13}C NMR (400 MHz, DMSO-d$_6$): δ (p.p.m.) 172.3, 166.4, 152.9, 148.7, 142.3, 138.8, 137.4, 133.8, 130.8, 127.5, 125.8, 125.2, 124.8, 120.4, 120.1, 119.3, 117.6, 112.4, 108.5, 107.3, 72.5, 47.9, 45.5, 40.1, 34.1, 31.1, 22.2, 18.1, 9.9, 8.7.

PPARγ Binding Assay

PPARγ competitive binding assay (Invitrogen) was performed according to the manufacturer's protocol. A mixture of 5 nM glutathione *S*-transferase fused with the PPARγ ligand binding domain (GST–PPARγ–LBD), 5 nM Tb-GST-antibody, 5 nM Fluormone

Pan-PPAR Green, and serial dilutions of compound beginning at 10 µM downwards was added to wells of black 384-well low-volume plates (Greiner) to a total volume of 18 µl. All dilutions were made in TR-FRET PPAR assay buffer. DMSO at 2% final concentration was used as a no-ligand control. Experiments were performed in triplicate and incubated for 2 h in the dark before analysis in Perkin Elmer ViewLux ultra HTS microplate reader. The FRET signal was measured by excitation at 340 nm and emission at 520 nm for fluorescein and 490 nm for terbium. The fold change over DMSO was calculated by 520 nm/490 nm ratio. Graphs were plotted in GraphPad Prism as fold change of FRET signal for each compound over DMSO-only control and EC_{50} calculated.

Cell-based transactivation assay

HEK293T cells (ATCC; cat# CRL-3216) were cotransfected in batch by adding 4.5 µg full-length human PPARγ2-pCMV-AN-DDK or full-length human mutant PPARγ2-F282A-pCMV-AN-DDK, with 4.5 µg 3x multimerized PPRE-luciferase reporter and 27 µl X-treme Gene 9 transfection reagent in serum-free Opti-mem reduced serum media (Gibco). After 18-h incubation at 37 °C in a 5% CO_2 incubator, transfected cells were plated in quadruplicate in white 384-well plates (Perkin Elmer) at a density of 10,000 cells per well. After replating, cells were treated with either DMSO only or the indicated compounds in increasing doses from 2 pM–10 µM. After 18-h incubation, treated cells were developed with Brite Lite Plus (Perkin Elmer) and read in 384-well Luminescence Perkin Elmer EnVision Multilabel plate reader. Graphs were plotted as fold change of treated cells over DMSO-treated control cells.

Crystallography

The PPARγ LBD was purified as previously reported using an N-terminal 6X polyhistidine tag [8]. Purified protein was concentrated to 10mg/mL and stored in 20mM Tris 8.0, 10mM NaCl, and 1mM TCEP. The SR1664 ligand bound structure was produced by co-crystallization and the SR1663 structure was produced by soaking apo PPARγ LBD T447F crystals with 10mM compound for 7 days. SR1664 was incubated with PPARγ LBD in a 10:1 (ligand:protein) ratio and the complex was isolated using an FPLC size exclusion column (Superdex™ 200, GE HealthSciences). Crystals of the SR1664-LBD complex were formed using a hanging drop vapor diffusion method; crystals formed within one week, were cubic in morphology, and grew to approximately 150microns in each dimension. Crystals were formed at 298 K using 1µL of well solution, 1µL of protein complex, and 500µL of well solution. The well solution consisted of 2M ammonium sulfate. Apo crystals of the PPARγ LBD were also grown by the vapor diffusion method at 298K and a hanging drop. Apo crystals were formed with 1µL of well solution, 1µL of protein complex, and 500µL of well solution; the well solution consisted of 1M sodium citrate and 0.1M HEPES 8.0. Apo crystals formed within 3 weeks, were cubic in morphology, and grew to approximately 300microns in each dimension. Apo crystals were soaked with SR1663 for 2 weeks at a final concentration of 1mM in the drop. Both SR1664 co-crystals and SR1663 soaked crystals were transferred to well solutions containing 15% ethylene glycol for use as a cryo-protectant. All data collection was performed with synchrotron radiation at SSRL beamline 11-1 at 100 K. 0.2° oscillations with 1.2s exposures were collected for a total of 240 degrees at a wavelength of 1.03Å. Data processing was carried out using HKL2000[27].

Both crystals were of space group C2 consistent with previously published PPARγ LBD crystal structures. Data processing and refinement parameters can be found in Table 1. The phase problem was overcome by means of molecular replacement using PDB:2Q59 (stripped of water molecules and ligands) as a search model[8]. Refinement was carried out using iterative rounds of refinement using phenix.refine followed by manual rebuilding in Coot[28] until R-factors converged. Molprobity was used for structure validation. Kicked 2F0-FC electron density maps were calculated for both ligands (Supplementary Figure 4).

The SR1664 crystal structure had 96.8% residues in favored Ramachandran positions. Both structures were deposited in the protein data bank: SR1664 as PDB:4R2U and SR1663 as PDB:4R65.

Hydrogen/Deuterium Exchange coupled with mass spectrometry

Solution-phase amide HDX experiments were carried out using a fully automated system as described previously[29]. 10 μM of HIS-PPARγ LBD protein (20mM KPO4 pH 7.4, 50mM KCl) was preincubated with 1:2 molar excess of compound. 5μl of protein solution was mixed with 20μl of D_2O-containing HDX buffer (20mM KPO4 pH 7.4, 50mM KCl) and incubated at 4 °C for 10s, 30s, 60s, 900s and 3,600s. Following on-exchange, unwanted forward or back exchange was minimized and the protein was denatured by dilution with 25uL of quench solution (0.1% v/v TFA in 3 M urea). Samples were then passed through an immobilized pepsin column (prepared in house [30]) at 200 μl min^{-1} (0.1% v/v TFA, 15 °C) and the resulting peptides were trapped on a C_8 trap column (Hypersil Gold, Thermo Fisher). The bound peptides were then gradient-eluted (5–50% CH_3CN w/v and 0.3% w/v formic acid) across a 2 mm × 50 mm C_{18} HPLC column (Hypersil Gold, Thermo Fisher) for 5 min at 4 °C. The eluted peptides were then subjected to electrospray ionization directly coupled to a high resolution Orbitrap mass spectrometer (Exactive, Thermo Fisher). Each HDX experiment was carried out in triplicate and the intensity weighted average m/z value (centroid) of each peptide isotopic envelope was calculated with in-house HDX Workbench software[31] (Supplementary Figure 5).

NMR spectroscopy

^{15}N PPARγ LBD protein was expressed and purified as described previously[32], with a final NMR buffer of 20mM KPO_4 (pH 7.0 or 7.4) 50mM KCl, 0.5mM EDTA. To prepare liganded samples, 8 μM protein was loaded ~1:1 with ligand dissolved in DMSO-d_6 and concentrated to 300 μM, followed by addition of 10% D_2O and 0.05% sodium azide. 2D [^1H,^{15}N]-TROSY-HSQC experiments were performed on a 700 MHz (^1H frequency) Bruker instrument at a calibrated temperature of 298K. Data were processed using Topspin 3.0 (Bruker) and analyzed using NMRViewJ (One Moon Scientific).

NCoR peptide recruitment assay

7.5nM Tb-α-HIS (Invitrogen), 10μM of ligand were incubated in complete TR-FRET PPAR assay buffer (Invitrogen) containing 7.5nM PPARγ protein (Invitrogen) or 7.5nM mutated PPARγ F282A. After 1 hour incubation at room temperature, 30μM NCoR NR box 2-1 peptide (THRLITLADHICQIITQDFAR) (LifeTein) was added and incubated for an additional 4 hours at room temperature, kept in the dark. The FRET signal was measured by

excitation at 340nm and emission at 520nm for fluorescein and 490nm for terbium in Perkin Elmer ViewLux ultra HTS microplate reader. The fold change over DMSO was calculated by 520nm/490nm ratio. Graphs were plotted in GraphPad Prism as fold change of FRET signal for each compound over DMSO-only control.

3T3-L1 Adipogenesis Assays

3T3-L1 cells (ATCC; cat# CL-173) were seeded at 50,000cells/mL in 12-well dish (Corning) with 1XDMEM (CellGro) containing 10%FBS (GIBCO) and incubated overnight at 37°C, 5%CO_2. The following day, cells were treated with 1μM compound and MDI cocktail consisting of 0.5mM 3-iso-butyl-1-methylxanthine, 1μM dexamethasone and 5μg/mL insulin. Following two days incubation, cells were treated with 1μM fresh compound diluted in 1XDMEM+10%FBS. After incubating for six days, cells were stained with oil red or harvested and lysed. RNA was extracted using RNeasy Mini Kit (Qiagen). Subsequently, cDNA was generated using High Capacity Reverse Transcription Kit (Applied Biosystems). Expression levels of PPAR-related genes were measured using Applied Biosystems 7500 Real-Time PCR system. Relative gene expression was calculated and plotted using GraphPad Prism Software.

Osteogenic Differentiation of Mesenchymal Stem Cells

MSCs were harvested from small volume aspirates of the iliac crest from healthy adult volunteers by the Center for Preparation and Distribution of Adult Stem Cells formerly at Tulane University School of Medicine (New Orleans, LA) and currently at Texas A&M Health Science Center (Temple, TX). Mononuclear cells were recovered from a ficoll (Ficoll-Plaque, Pharmacia; Peapack, NJ) gradient, washed using Hank's balanced salt solution (HBSS) and centrifuged at 500g for 10 min. Mononuclear cells were then plated at 5000 cells/cm2 and cultured in complete culture medium (CCM) consisting of alpha-minimum essential medium (α-MEM) supplemented with 2 mM L-glutamine, 17% fetal bovine serum (FBS) (HyClone, Logan, UT, http://www.hyclone.com) 100 U/ml of penicillin, and 100 μg/ml of streptomycin at 37°C in a humidified incubator with 5% CO_2. After 24 hours the non-adherent cells were removed and adherent cells were cultured to 70% confluence with media changes every 2–3 days. Cells were then harvested using 0.2% trypsin-EDTA and secondary cultures were routinely plated at 500–1000 cells/cm2 and expanded as described above. Osteogenic differentiation was performed by culturing MSCs in osteogenic induction media (OIM; DMEM low glucose supplemented with 10% fetal bovine serum, 10 mM β-glycerophosphate, 50 μg/mL L-ascorbic acid 2-phosphate1% penicillin/streptomycin) containing vehicle or compounds for 15 days with media changes every 2–3 days.

In experiments involving PPARγ knockdown, OIM was added 24 hours after siRNA (10 nM) transfection. After 15 days of differentiation, cells were washed with PBS, incubated in 10% neutral buffered formalin for 1 hour at room temperature, washed with deionized water and stained with Alizarin Red S for 20 minutes at room temperature. Monolayers were then rinsed 3x with de-ionized water until clear, washed with PBS, stain was then extracted with 10% (w/v) cetylpyridinium chloride in 10 mM sodium phosphate, pH 7.0 for 15 minutes at room temperature, and the amount of extracted dye quantified spectroscopically at 562 nm.

Spectroscopic analysis performed using a SpectraMax® M5e Multi-Mode Microplate Reader (Molecular Devices, LLC.) and images acquired using a Leica DMI3000B upright fluorescent microscope attached to a DFC295 digital camera (Micro Optics of Florida, Inc., Davie, FL, http://www.microopticsfl.com). RNA was isolated from cell monolayer after 5 days of differentiation for gene expression studies.

Gene expression analysis

Total RNA was isolated from cells or tissues using TRIzol reagent (Invitrogen). The RNA was reverse-transcribed using the ABI reverse transcription kit. Quantitative PCR reactions were performed with SYBR green fluorescent dye using an ABI9300 PCR machine. Relative mRNA expression was determined by the $-C_t$ method normalized to GAPDH or TBP levels. The sequences of primers used in this study are found in Supplementary Table 2.

Animals

All animal experiments were performed according to procedures approved by Scripps-Florida IACUC Committee. Male C57BL/6J mice were purchased from the Jackson Laboratory (7-week-old) and fed a regular chow diet through experiments. The mice were dosed by oral gavage once daily with 5 mg kg^{-1} rosiglitazone or 20 mg kg^{-1} SR2595 for 21 days. For insulin tolerance tests, mice were fasted overnight before i.p. Injection of 0.75U/kg insulin (Sigma). Glucose was then measured by tail vein bleeds at the indicated intervals using an OneTouch Ultra2 glucometer. Plasma insulin concentration was determined by ELISA (Millipore mouse/rat insulin. cat # EZRMI-13K).

Supplementary Material

Refer to Web version on PubMed Central for supplementary material.

ACKNOWLEDGEMENTS

References

1. Viccica G, Francucci CM, Marcocci C. The role of PPARgamma for the osteoblastic differentiation. Journal of endocrinological investigation. 2010; 33:9–12. [PubMed: 20938219]

2. Aubert RE, Herrera V, Chen W, Haffner SM, Pendergrass M. Rosiglitazone and pioglitazone increase fracture risk in women and men with type 2 diabetes. Diabetes, obesity & metabolism. 2010; 12:716–721.

3. Rangwala SM, Lazar MA. The dawn of the SPPARMs? Science's STKE : signal transduction knowledge environment. 2002; 2002:pe9.

4. Higgins LS, Depaoli AM. Selective peroxisome proliferator-activated receptor gamma (PPARgamma) modulation as a strategy for safer therapeutic PPARgamma activation. The American journal of clinical nutrition. 2010; 91:267S–272S. [PubMed: 19906796]

5. Choi JH, et al. Anti-diabetic drugs inhibit obesity-linked phosphorylation of PPARgamma by Cdk5. Nature. 2010; 466:451–456. [PubMed: 20651683]

6. Choi JH, et al. Antidiabetic actions of a non-agonist PPARgamma ligand blocking Cdk5-mediated phosphorylation. Nature. 2011; 477:477–481. [PubMed: 21892191]

7. Akune T, et al. PPARgamma insufficiency enhances osteogenesis through osteoblast formation from bone marrow progenitors. The Journal of clinical investigation. 2004; 113:846–855. [PubMed: 15067317]

8. Bruning JB, et al. Partial agonists activate PPARgamma using a helix 12 independent mechanism. Structure. 2007; 15:1258–1271. [PubMed: 17937915]

9. Walkey CJ, Spiegelman BM. A functional peroxisome proliferator-activated receptor-gamma ligand-binding domain is not required for adipogenesis. J Biol Chem. 2008; 283:24290–24294. [PubMed: 18622018]

10. Rocchi S, et al. A unique PPARgamma ligand with potent insulin-sensitizing yet weak adipogenic activity. Molecular cell. 2001; 8:737–747. [PubMed: 11684010]

11. Miles PD, Barak Y, Evans RM, Olefsky JM. Effect of heterozygous PPARgamma deficiency and TZD treatment on insulin resistance associated with age and high-fat feeding. American journal of physiology. Endocrinology and metabolism. 2003; 284:E618–E626. [PubMed: 12556354]

12. Miles PD, Barak Y, He W, Evans RM, Olefsky JM. Improved insulin-sensitivity in mice heterozygous for PPAR-gamma deficiency. The Journal of clinical investigation. 2000; 105:287–292. [PubMed: 10675354]

13. Shiau AK, et al. The structural basis of estrogen receptor/coactivator recognition and the antagonism of this interaction by tamoxifen. Cell. 1998; 95:927–937. [PubMed: 9875847]

14. Taygerly JP, et al. Discovery of INT131: a selective PPARgamma modulator that enhances insulin sensitivity. Bioorganic & medicinal chemistry. 2013; 21:979–992. [PubMed: 23294830]

15. Carmona MC, et al. S 26948: a new specific peroxisome proliferator activated receptor gamma modulator with potent antidiabetes and antiatherogenic effects. Diabetes. 2007; 56:2797–2808. [PubMed: 17704298]

16. Yue L, et al. The conserved residue Phe273(282) of PPARalpha(gamma), beyond the ligand-binding site, functions in binding affinity through solvation effect. Biochimie. 2005; 87:539–550. [PubMed: 15935279]

17. Itoh T, et al. Structural basis for the activation of PPARgamma by oxidized fatty acids. Nature structural & molecular biology. 2008; 15:924–931.

18. Tsukahara T, et al. Phospholipase D2-dependent inhibition of the nuclear hormone receptor PPARgamma by cyclic phosphatidic acid. Molecular cell. 2010; 39:421–432. [PubMed: 20705243]

19. Zaytseva YY, Wallis NK, Southard RC, Kilgore MW. The PPARgamma antagonist T0070907 suppresses breast cancer cell proliferation and motility via both PPARgamma-dependent and -independent mechanisms. Anticancer research. 2011; 31:813–823. [PubMed: 21498701]

20. Seargent JM, Yates EA, Gill JH. GW9662, a potent antagonist of PPARgamma, inhibits growth of breast tumour cells and promotes the anticancer effects of the PPARgamma agonist rosiglitazone, independently of PPARgamma activation. British journal of pharmacology. 2004; 143:933–937. [PubMed: 15533890]

21. Burton JD, Goldenberg DM, Blumenthal RD. Potential of peroxisome proliferator-activated receptor gamma antagonist compounds as therapeutic agents for a wide range of cancer types. PPAR research. 2008; 2008:494161. [PubMed: 18779871]

22. Ryan KK, et al. A role for central nervous system PPAR-gamma in the regulation of energy balance. Nature medicine. 2011; 17:623–626.

23. Nakano R, et al. Antagonism of peroxisome proliferator-activated receptor gamma prevents high-fat diet-induced obesity in vivo. Biochemical pharmacology. 2006; 72:42–52. [PubMed: 16696951]

24. Liu C, et al. PPARgamma in vagal neurons regulates high-fat diet induced thermogenesis. Cell metabolism. 2014; 19:722–730. [PubMed: 24703703]

25. Cheng Y, et al. Lysophosphatidic acid-induced arterial wall remodeling: requirement of PPARgamma but not LPA1 or LPA2 GPCR. Cellular signalling. 2009; 21:1874–1884. [PubMed: 19709640]

26. Krause U, et al. Pharmaceutical modulation of canonical Wnt signaling in multipotent stromal cells for improved osteoinductive therapy. Proceedings of the National Academy of Sciences of the United States of America. 2010; 107:4147–4152. [PubMed: 20150512]

27. Otwinowski Z, Minor W. Processing of X-ray diffraction data collected in oscillation mode. Method Enzymol. 1997; 276:307–326.

28. Emsley P, Cowtan K. Coot: model-building tools for molecular graphics. Acta Crystallogr D. 2004; 60:2126–2132. [PubMed: 15572765]

29. Chalmers MJ, et al. Probing protein ligand interactions by automated hydrogen/deuterium exchange mass spectrometry. Analytical chemistry. 2006; 78:1005–1014. [PubMed: 16478090]

30. Chalmers MJ, Busby SA, Pascal BD, Southern MR, Griffin PR. A two-stage differential hydrogen deuterium exchange method for the rapid characterization of protein/ligand interactions. Journal of biomolecular techniques : JBT. 2007; 18:194–204. [PubMed: 17916792]

31. Pascal BD, et al. HDX workbench: software for the analysis of H/D exchange MS data. J Am Soc Mass Spectrom. 2012; 23:1512–1521. [PubMed: 22692830]

32. Hughes TS, et al. An alternate binding site for PPARgamma ligands. Nature communications. 2014; 5:3571.

33. Tremain N, et al. MicroSAGE analysis of 2,353 expressed genes in a single cell-derived colony of undifferentiated human mesenchymal stem cells reveals mRNAs of multiple cell lineages. Stem Cells. 2001; 19:408–418. [PubMed: 11553849]
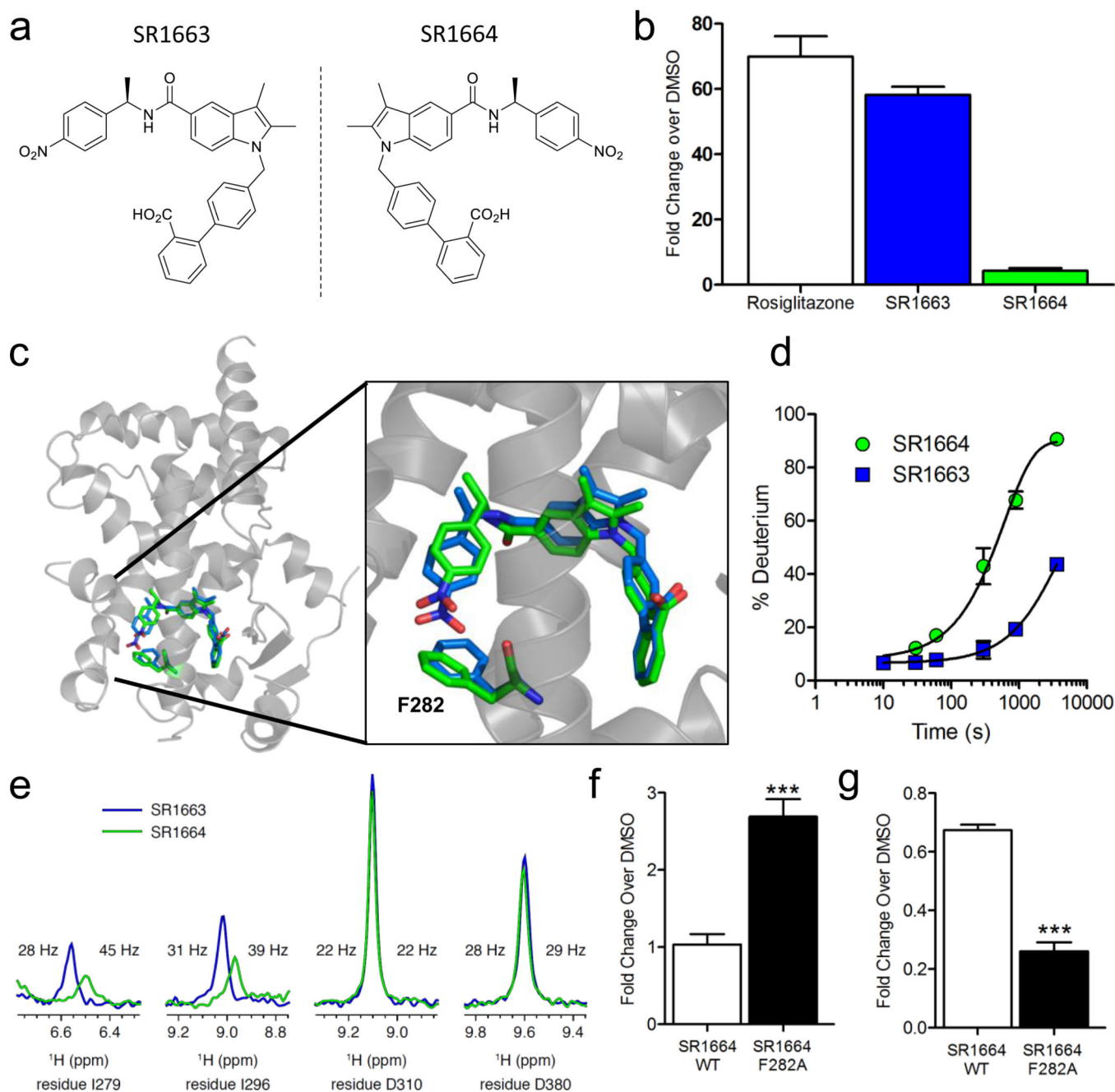
Figure 1. Structure Activity Relationship Around Enantiomers SR1663 & SR1664
(**a**) Chemical structures of SR1664 and R-enantiomer SR1663. (**b**) Transcriptional activity of a PPARγ-Gal4:UAS-Luciferase promoter-reporter assay in HEK293T cells with 1 μM ligand. (**c**) Alignment of PPARγ:SR1663 (blue) and PPARγ:SR1664 (green) cocrystal structures. Zoomed panel highlights stereo-specific interaction with residue F282. (**d**) HDX buildup curves of PPARγ LBD helix 3 peptide (*IRIFQGCQ*) containing F282 in the presence of SR1663 and SR1664. (**e**) Extracted 1D plots from 2D [^{1}H,^{15}N]-TROSY-HSQC NMR data for PPARγ LBD in the presence of SR1663 or SR1664; half-height resonance line widths are indicated. (**f**) Transcriptional activity of wild type vs. F282A PPARγ in

PPARγ:PPRE-Luciferase promoter-reporter assay with 1uM SR1664 in HEK293T cells. (**g**) Wild type vs F282A PPARγ:NCoR NR Box 1 peptide affinity with 1uM SR1664 in TR-FRET assay. Error bars, s.e.m; one-way ANOVA, Dunnett's *post hoc* test *P < 0.05, ** < 0.01, ***P < 0.001.
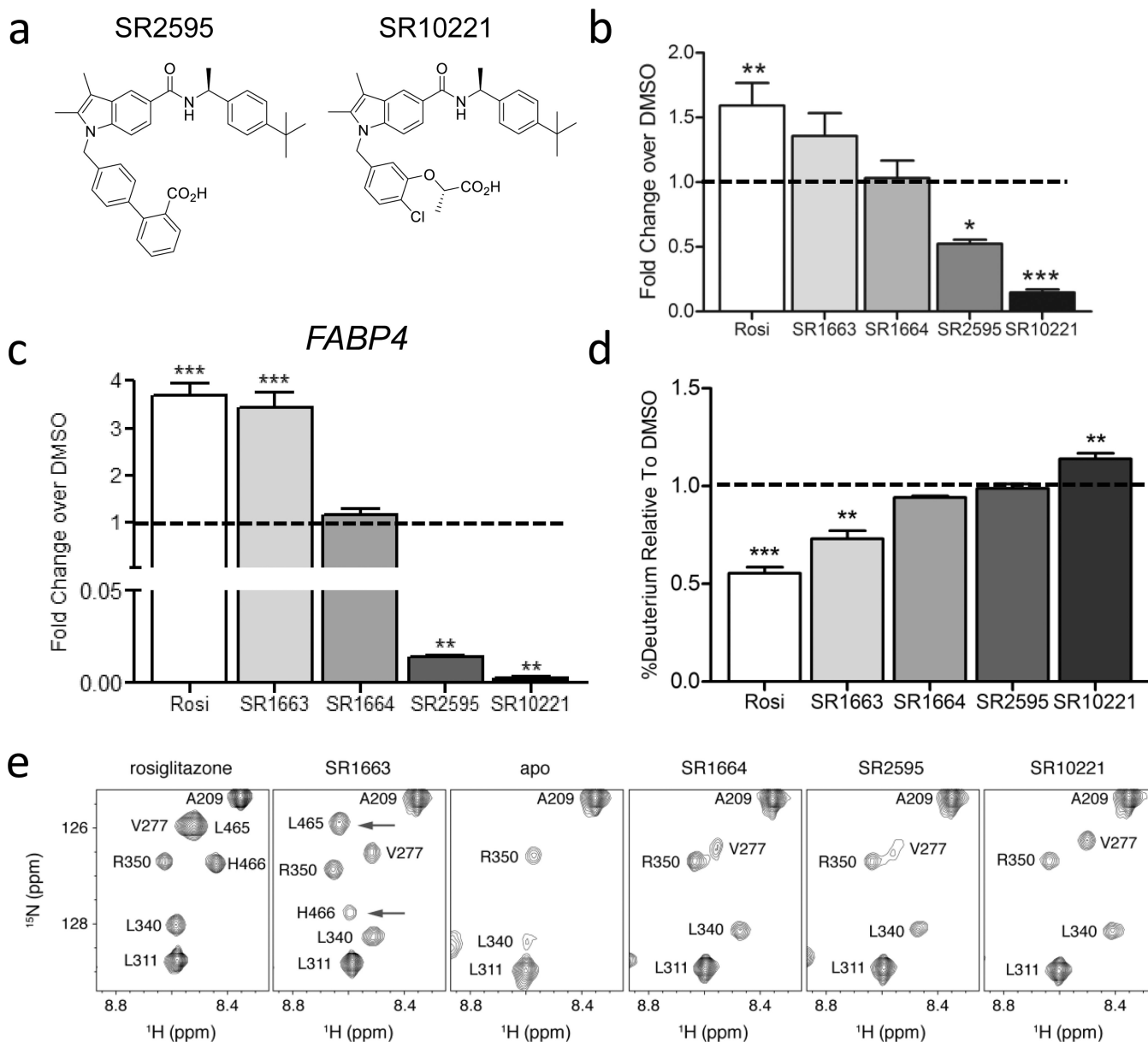
Figure 2. Structure Guided Design of PPARγ Inverse Agonists
(**a**) Chemical structures of SR2595 and SR10221. (**b**) Transcriptional activity of a PPARγ:PPRE-Luciferase promoter-reporter assay in 1uM treated HEK293T cells (n=3). (**c**) qPCR analysis of mRNA extracts from 1μM treated, differentiated 3T3-L1 adipocytes for adipogenic marker *FABP4* (n=3). (**d**) HDX of PPARγ helix 12 peptide SLHPLLQEIYKDLY (PPARγ1 residues 492-505) after 30 second D_2O incubation in the presence of ligand relative to DMSO control (n=3). (**e**) 2D [^1H,^{15}N]-TROSY-HSQC NMR data for PPARγ LBD in the presence of the indicated ligands; arrows indicate resonances near helix 12 that are stabilized by rosiglitazone and SR1663 only. Error bars, s.e.m; one-way ANOVA, Dunnett's *post hoc* test *P < 0.05, ** < 0.01, *** P < 0.001.
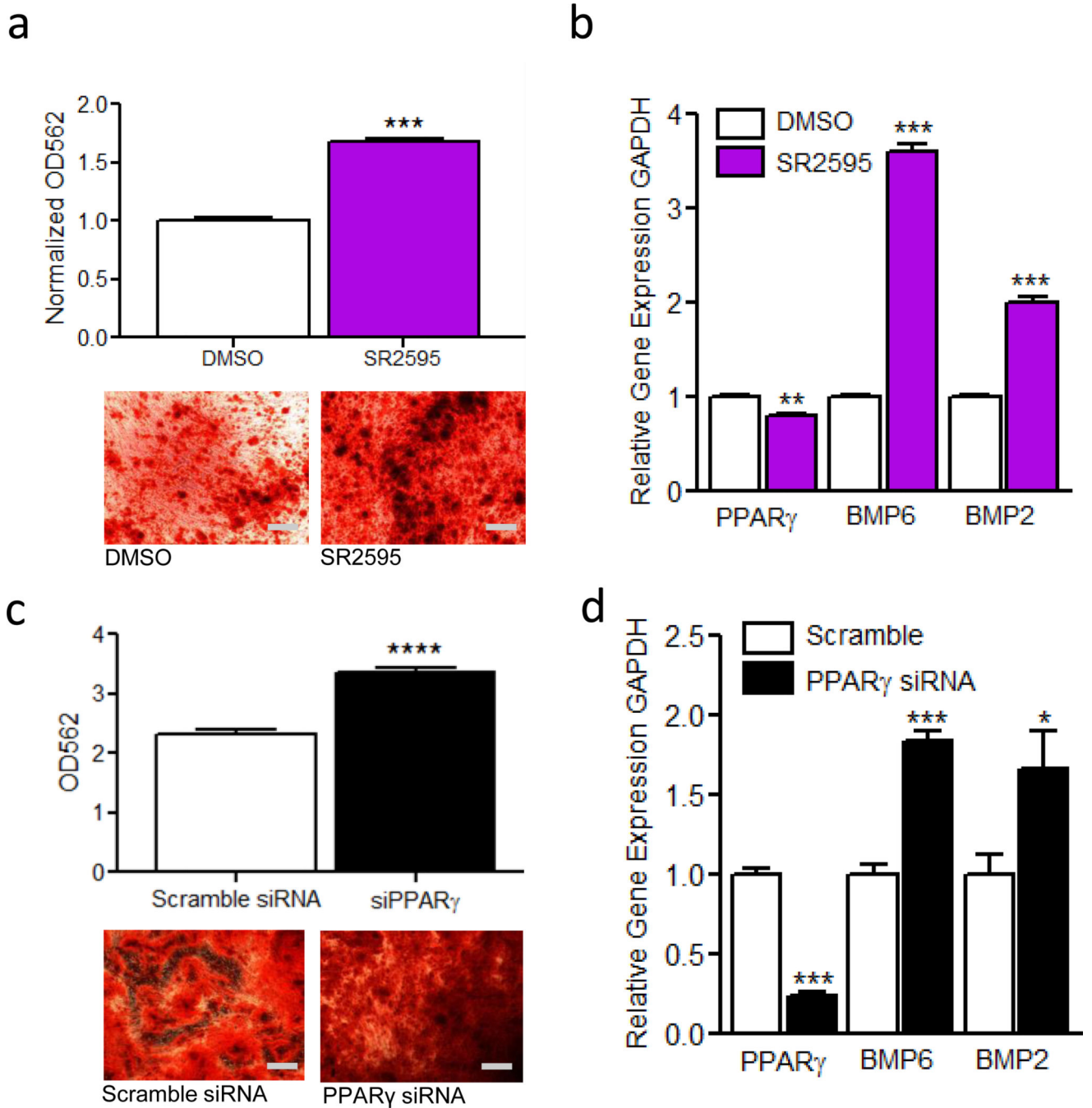
Figure 3. Pharmacological Repression of PPARγ Promotes Osteogenesis

(**a**) Alizarin red staining and quantification of MSCs treated with 1 μM SR2595 (n=3), scale bar is 1mm. (**b**) qPCR analysis of mRNA extracts from 1 μM SR2595 treated MSCs (n=3). (**c**) Alizarin red staining and quantification of MSCs treated with PPARγ siRNA (n=3), scale bar is 1mm. (**d**) qPCR analysis of mRNA extracts from siRNA treated MSCs (n=3). Error bars, s.e.m; one-way ANOVA, Dunnett's *post hoc* test *P < 0.05, ** < 0.01, *** P < 0.001.

Table 1

Data collection and refinement statistics

	SR1663	SR1664
Data collection		
Space group	C2	C2
Cell dimensions		
a, b, c (Å)	93.2, 61.9, 119.2	89.6, 63.7, 118.8
a, b, g (°)	90.0, 103.4, 90.0	90.0,103.4,90.0
Resolution (Å)	41.1-2.3 (2.3-2.4) [*]	31.5-2.3 (2.3-2.4)
R_{merge}	3.2 (42.6)	9.4 (53.2)
I / σI	29.9 (2.3)	6.2 (1.7)
Completeness (%)	97.8 (98.1)	97.0 (79.4)
Redundancy	4.2 (4.2)	3.7 (3.5)
Refinement		
Resolution (Å)	41-2.3	50-2.3
No. reflections	28903 (1448)	28278 (2249)
Rwork/ Rfree	17.1/23.3	
No. atoms		
Protein	4062	4019
Ligand/ion	82	82
Water	111	173
B-factors		
Protein	79.2	53.5
Ligand/ion	94.1	61.3
Water	74.6	56.2
R.m.s. deviations		
Bond lengths (Å)	0.009	0.010
Bond angles (°)	1.12	1.26

[*] Data sets were collected from 1 crystal.

[*] Values in parentheses are for highest-resolution shell.